IV International Conference on Computational Methods for Coupled Problems in Science and Engineering
COUPLED PROBLEMS 2011
M. Papadrakakis, E. Oñate and B. Schrefler (Eds)

PROCESS MODELLING OF LINEAR FRICTION WELDING (LFW) BETWEEN AA2124/SIC$_P$ COMPOSITE AND UNREINFORCED ALLOY

X. SONG[*], N. BAIMPAS[*], S. HARDING[†] AND A. M. KORSUNSKY[*]

[*] Department of Engineering Science, Parks Road
University of Oxford,
Oxford, UK OX1 3PJ
e-mail: xu.song@eng.ox.ac.uk, alexander.korsunsky@eng.ox.ac.uk,
http://www.eng.ox.ac.uk/solidmech/

[†] Combustion Systems - Engineering
WH-45, Rolls Royce Plc
Bristol, UK BS34 7QE
email: stephen.harding@rolls-royce.com, http://www.rolls-royce.com/

Key words: Finite Elements (FE), Linear Friction Welding (LFW), Metal Matrix Composite (MMC), Fully coupled thermo-mechanical process modelling

Abstract. In the present study, the Linear Friction Welding (LFW) process between a bar of Metal Matrix Composite (MMC) AMC225xe (AA2124 with 25% SiC particulate reinforcement) and a bar of unreinforced base alloy was simulated using the commercial finite element package ABAQUS^{TM}. Fully coupled implicit thermo-mechanical analysis procedure was employed, with semi-automatic re-meshing using Python scripting and output database scripting methods for extracting deformed configurations. Due to the large deformation near the weld region, multiple analyses were carried out between each re-meshing stage in order to limit the element distortion. Comparison of the simulation results with the experimental data collected during welding, and with post-weld optical section micrograph has shown satisfactory agreement.

1 INTRODUCTION

Metal Matrix Composites (MMCs) are a class of materials that typically contain reinforcement particles or fibres dispersed in a continuous metallic matrix. Over the past few decades, significant effort has been dedicated to developing MMCs with better physical and mechanical properties compared to monolithic metals. The synergy between the properties of the matrix (usually a light alloy based on Al, Ti or Mg) and the reinforcement (usually a hard ceramic oxide, carbide, or nitride) allows the MMCs to exceed the parent material's performance [1]. MMCs based on aluminium alloys form a class of attractive light-weight materials possessing a good combination of high stiffness and strength. The incorporation of stiff and hard reinforcement in the form of fibres or particles leads to a significant increase in the overall elastic modulus. Strength is also improved due to a variety of mechanisms, including grain refinement and the creation of additional obstacles to dislocation movement.

AA2124 is a wrought aluminium alloy widely used in the aerospace industry, e.g. fuselage, fuel tanks etc. It possesses a good combination of mechanical properties: relatively high stiffness and high strength, low density, and good resistance to fatigue crack growth. MMCs based on the AA2124 alloy usually use silicon carbide (SiC) particle reinforcement, due to the good interfacial bond that can be formed with the matrix.

Despite the several advantages over conventional alloys, a significant limitation to the industrial application of AMCs is posed by the problems that arise in conventional joining techniques, such as segregation and degradation (fracture) of the reinforcement phase. Recently, linear friction welding has been successfully applied to join aluminium alloy based MMCs. One of the crucial advantages of the LFW joining technique is that it avoids melting and solidification [2]: it is a solid state joining process in which the bonding of two parallel-edged components is completed by their relative reciprocating motion under the action of steady axial compressive force. During the process, significant heat is generated by the friction at the component interface, resulting in the continued displacement of plastically deformed material [3-7]. This reciprocal motion and the very large attendant strains, together with the complex interaction between the thermal and mechanical behaviour of components makes the task of modelling the process somewhat of a challenge. Previous attempts have been made to carry out Finite Element (FE) simulation of the LFW process between two components made from the same Ti alloy, leading to limited success in capturing the temperature field evolution [7, 8]. To the best of the authors' knowledge, no work has been reported to date on simulating LFW of aluminium alloys or aluminium-based composites, particularly for the case of joining two blocks with different material properties.

Below we describe the simulation setup and report the comparison of the optimised model output with observations.

2 THE FINITE ELEMENT SIMULATION

2.1 The LFW process description

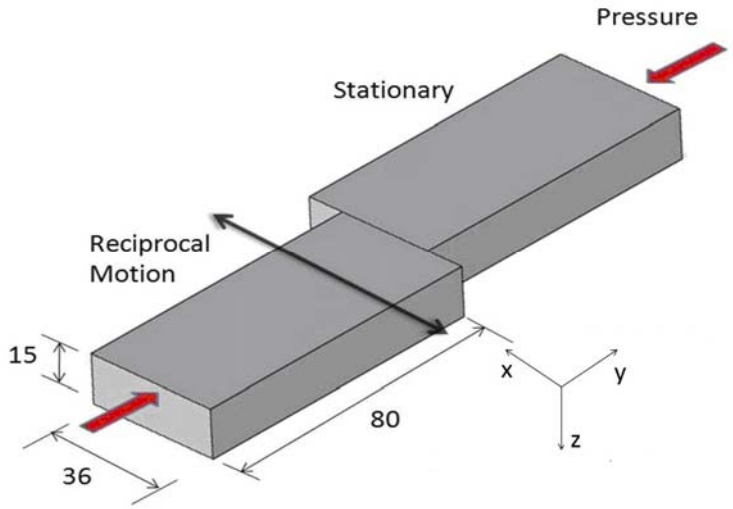

Figure 1: Illustration of the AA2124/MMC linear friction welding arrangement, and the coordinate system used.

In order to simulate the entire linear friction welding process, the detailed parameters of the welding process are required. In the present study we used the data collected during Linear Friction Welding of AA2124/AMC225xe performed at TWI (The Welding Institute, Cambridge, UK). The schematic illustration of the welding setup can be seen in Figure 1, and the details of the welding process parameters are given in Table 1 and Figure 2.

Table 1: Linear friction welding process parameters

Joint	Force (kN)	Pressure (MPa)	Frequency (Hz)	Amplitude (mm)	Burn-off (mm)	Piece Initial Length (mm)	Weldment Length (mm)	Total Upset (mm)
AA2124/ AMC225xe	85	157	50	2	2	80	150.94	9.06

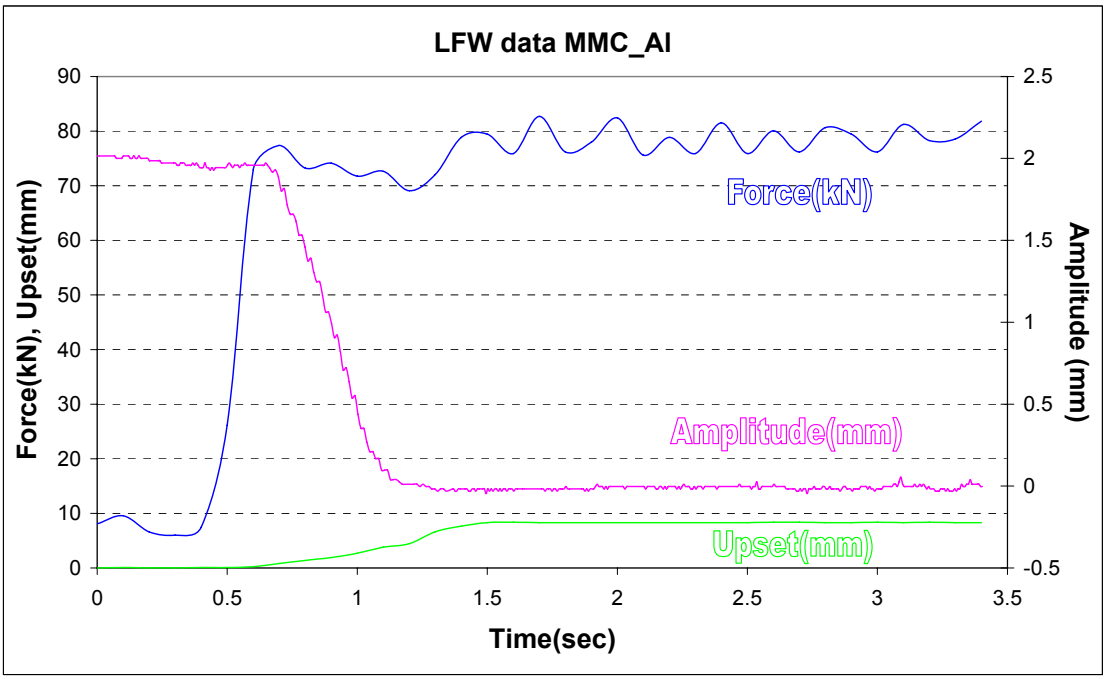

Figure 2: Plots of time history of the applied force, amplitude and upset during LFW process

In Table 1, total upset means the total axial shortening of the two components after welding, while burn-off indicates the critical initial shortening at which the LFW control system begins to reduce the oscillation amplitude. In the simulation, one bar of the assembly was maintained stationary, while the other was subjected to oscillatory movement along the *y*-direction whilst experiencing a compressive force in the *x*-direction applied at the top end of the bar. When the axial shortening reached 2mm, when the corresponding time was ~0.65s in Figure 2, the oscillation amplitude was triggered to reduce in a linear ramp that reached zero in 0.5s, which also corresponded to the time interval for observation made in the course of the experiment (Figure 2).

2.2 Setup of 2D LFW simulation

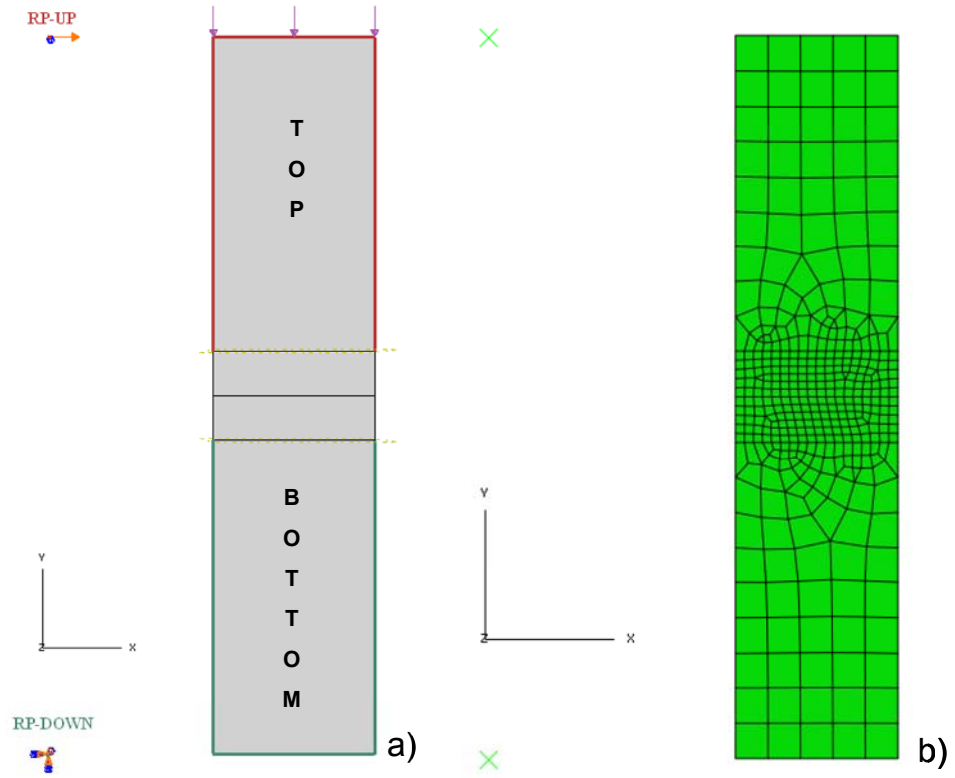

Figure 3: a) 2D model setup with boundary conditions and loads; b) 2D mesh with fine and coarse mesh regions

For the purposes of the current study, a 2D model was created with the exact in-plane dimensions of the specimens, i.e. the width of 36mm and length of 80mm for each bar (Figure 3). As illustrated in the Figure, the bottom bar was encastre, whilst the top bar had time-varying displacement boundary conditions applied to represent the oscillatory movement during the welding process. Two Reference Points (RP) were created in the model, for the following purposes: 1) to apply fixed or moving displacement boundary conditions, by linking the RPs through input command "*Equations" with the specific edges of the model, highlighted in colour in Figure 3a; 2) to act as a sensor through a user subroutine (UEL) for measuring the current weld upset. When a critical user-defined upset distance is reached or exceeded, the UEL calls the utility routine XIT to trigger re-meshing and to ensure that the elements are not excessively distorted; 3) to play the role of information channel between the input file and various subroutines at the beginning of each re-mesh analysis step, so that the total run time information can be made available for the user-defined subroutine UAMP that defines the amplitudes of oscillation and pressure. In this way, the kinematic aspects of the bars being joined can be fully monitored and controlled via the respective RPs.

The LFW process model developed in the present study follows a nonlinear, quasi-static, thermo-mechanically coupled analytical framework. Each analysis step in the simulation sequence represented a single fully coupled temperature-displacement calculation. The exact duration of the step was not known a priori, but was in fact controlled by the user element subroutine UEL.

The key aspect of the implementation that was crucial for successful completion of the simulation was the re-meshing capability. During LFW, large deformation occurs in the near the weld region, namely, local shearing, forging and flash formation. If a single mesh were used, no matter how fine, element distortion would accumulate and soon render the calculation impossible. To limit element distortion, re-meshing had to be triggered when certain criteria were fulfilled. The procedure was automated through the use of Python scripts. To capture the significant changes in the component shape, the capabilities of ABAQUS/CAE were used to extract the outer contour of the bars, re-seed the surface, and create the new mesh in the automatic mode. In each bar, the mesh was divided into two regions (see Figure 3b). Smaller elements were used in the region near the bond line, and also for the materials forming the flash.

To describe the contact conditions, two types of contact interactions were defined: weld contact and self-contact. The weld contact was described by a pair of interactions that was symmetrical, in the following sense. The first interaction defined the bottom surface of the top bar as the *master* surface and the top surface of the bottom bar as the *slave* surface. In the second interaction definition this master-slave relationship was reversed. This "balanced master-slave" arrangement ensures more accurate and stable description of the contact pressure at the weld interface and avoids "hourglass" effects. Furthermore, it was combined with a softened contact interaction description in order to promote the re-distribution of the contact pressure between nodes lying along and to both sides of the interface between the two bars being joined.

The other type of contact interaction was introduced to address the possibility of self-contact that may cause problems during re-meshing. The *Part2DGeomFrom2DMesh* command was used to generate the new, current configuration geometry. This is achieved by performing curve-fit operations, and these in turn may lead to self-intersections of the boundary, with consequent invalid part topology and meshing failure. To overcome this problem, a softened contact model was used that introduced a normal pressure even for a small separation distance (0.01 mm). The separation distance was kept as small as practical to avoid introducing non-physical assumptions into the contact behaviour.

2.3 Material properties

The material of the top and bottom bars was AMC225xe and AA2124, respectively. The inelastic deformation response of both materials was described by constitutive laws that incorporated temperature and strain rate dependence of yield stress. The strain rate dependence was defined by the Johnson-Cook law where the prevailing exponential coefficient used was C = 0.0083 [9]. The temperature dependence of the other relevant physical and mechanical properties was found from the ASM Metals Handbook [10]. The values used in the simulation are given in Table 2 and 3. It is worth noting that the temperature dependence of the yield stress exerts crucial influence on the LFW process, while the strain rate-dependence of the yield stress greatly influences the model convergence. For a simulation that is stable and realistic, correct definitions of the temperature and strain rate dependence of the properties of both AA2124 and AMC225xe materials are of crucial importance.

Table 2: Material properties for AA2124

Temperature (°C)	Yield Stress (MPa)	Elongation	UTS (MPa)
24	450	8%	485
150	395	10%	415
205	340	13%	365
260	240	17%	270
315	145	23%	160
370	69	35%	76
Density (kg/m)	Thermal Conductivity (W/m·K)	Specific Heat (J/kg·K)	Young's Modulus (GPa)
2770	191	882	71

Table 3: Material proerties for AMC225xe

Temperature (°C)	Yield Stress (MPa)	Elongation	UTS (MPa)
20	480	5%	650
25	480	5%	650
150	321	9%	428
200	276	18%	358
260	102	34%	200
350	48	45%	65
Density (kg/m)	Thermal Conductivity (W/m·K)	Specific Heat (J/kg·K)	Young's Modulus (GPa)
2880	150	836	115

3 RESULTS AND DISSCUSSION

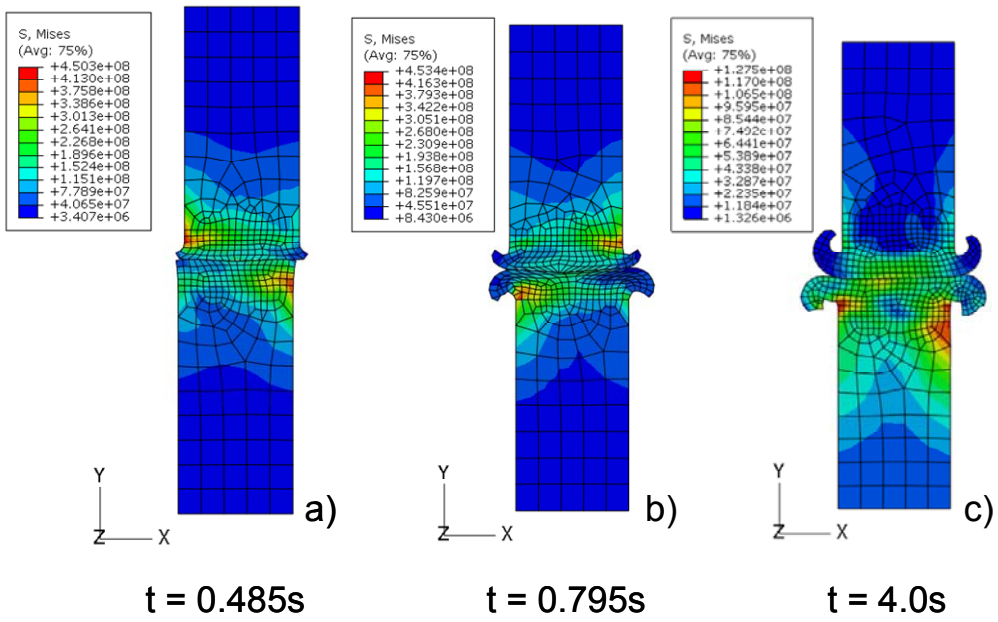

Figure 4: Von Mises stress contours in the specimen at different frame time: a) 0.485s, b) 0.795s and c) 4.0s

The LFW simulation presented here had the total duration of 4s, and burn-off time 0.85s. The oscillation amplitude was ramped down to zero at a time close to 1.15s. At 3.5s the applied load began to decrease, and at the target time of 4s the compressive load was reduced to zero.

The von Mises stress contours at different stages of the simulation are shown in Figure 4. The sequence provides an illustration of how the process evolves and what significant shape changes occur. They involve the "squeezing out" of the material from the weld zone and into the flash. It is seen in Figure 4a that at ~0.5s significant flash generation and axial shortening (upset) begin. At the time of ~0.8s, greater amount of flash was generated in both bars, with some noticeable asymmetry (right to left), and with significantly more flash produced on the AA2124 side. This remains true at 4.0s (end of the process, Figure 4c): most of the flash is seen in the unreinforced alloy side of the weldment, while only a relatively thin layer of highly curved AMC flash can also be found.

Figure 4c represents the distribution of von Mises stress within the assembly at the end of the process. At this stage the externally applied compressive force is already removed, so the residual stress state is being considered. As expected, a higher level of residual stress is found in the softer of the two bars being joined.

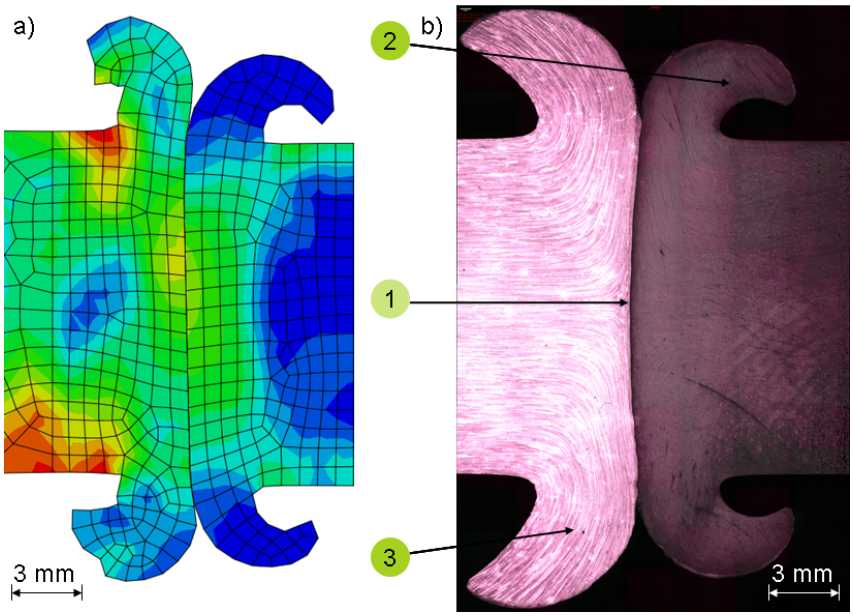

Figure 5: Flash geometry a) in the model and b) in the experiment in LFW of AA2124/AMC225xe

One possibility of validating the process model is to compare the predicted post-weld flash shape with the optical section micrograph. Figure 5 shows, on the same scale, the comparison of the flash geometry between the FE model and experiment (LFW bond region observed under an optical microscope) . The shapes of the flash for the AMC225xe material obtained

from the model and experiment appear almost identical, with both the flash thickness and curvature (Region 2 in Figure 5b) captured well. The flash shape for the unreinforced alloy AA2124 obtained in the model is somewhat similar from the observation, although the flash thickness once again appears to be captured correctly (see Region 3). The model also captures correctly the gentle curvature of the bond line in Region 1, with the region occupied by the relatively hard MMC appears convex, and concave for the softer AA2124 alloy.

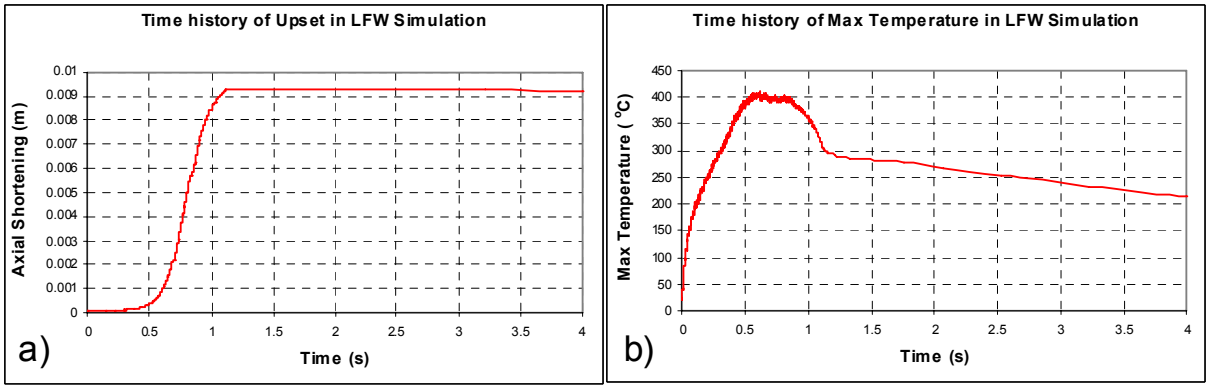

Figure 6: a) Time history of the axial shortening (upset) in the LFW simulation; b) Time history of the maximum temperature in the LFW simulation

Model post-processing was also developed in order to extract the upset and maximum temperature across the entire sequence of simulation steps. Figure 6 illustrates the time history of the model upset and maximum temperature during the LFW simulation. It is worth noting that the final upset of the model (9.36mm) is quite close to the experimental value (9.06mm). Furthermore, at the time of 0.65s, the upset predicted by the model is ~2mm, i.e. in precise agreement with the burn-off value when the oscillation amplitude started to decline. It is worth pointing out for clarity that the ramping down of oscillation amplitude in the simulation is time-triggered at t=0.65s. In contrast, in the experiment it is the burn-off reaching u=2mm that acts as a trigger for reducing oscillatory the amplitude.

It is also worth noting that the maximum process temperature within the model fell into the logical range, not exceeding the solidus temperature (502˚C) yet close to that of the forging (400˚C).

4 CONCLUSIONS

In the present study, a successful simulation is reported of the LFW process between unreinforced aluminum alloy AA2124 and Metal Matrix Composite AMC225xe that is based on the same alloy as the matrix and is reinforced with particulate SiC. The fully coupled implicit thermo-mechanical analysis procedure is described, with semi-automatic re-meshing to control element distortion. The simulation provided satisfactory agreement with the records of process parameters taken during welding, i.e. compressive force required for forging, burn-off and total upset. Further validation of predictive capability in terms of the mechanical behaviour of joints requires comparing the residual stresses from the simulation with experimental measurements carried out on the weldments e.g. by diffraction. This work is currently under way.

REFERENCES

[1] Clyne, T.W. and Withers, P.J., *Introduction to metal matrix composites*, Cambridge University Press, (1993).

[2] Jun, T.S., Rotundo, F., Ceschini. L., and Korsunsky, A.M. A study of residual stresses in Al/SiCp linear friction weldment by energy-dispersive neutron diffraction. *Key. Eng. Mater.* (2008) **385-387**: 517-520.

[3] Vairis, A., and Frost, M., High frequency linear friction welding of a titanium alloy. *Wear* (1998) **217**:117-131.

[4] Li, W.Y., Ma T.J. and Li, J.L., Numerical simulation of Linear Friction Welding of titanium alloy: Effects of processing parameters. *Mater. Design*, (2010) **31**: 497-1507.

[5] Wanjara, P., Jahazi, M., Thermal-Phase Transformation Modelling and Neural Network Analysis of Friction Welding of Non-Circular Eutectoid Steel Components. *Metall. Mater. Trans. A*, (2005) **36**: 2149-2164.

[6] Daymond, M.R. and Bonner, N.W., Measurement of strain in a titanium linear friction weld by neutron diffraction, *Physica B*, (2003) **325**: 130-137.

[7] Vairis, A., and Frost, M., Modelling the linear friction welding of titanium blocks, *Mater. Sci. Engng. A*, (2000) **292**: 8-17.

[8] Müller, S., Rettenmayr, M., Schneefeld, D., Roder O. and Fried W., FEM simulation of the linear friction welding of titanium alloys, *Comp. Mat. Sci.*, (2010) **48**: 749–758.

[9] Schmidt, H. and Hattel, J., A local model for the thermomechanical conditions in friction stir welding, *Modelling Simul. Mater. Sci. Eng.*, (2005) **13**: 77–93

[10] Cubberly, W.H. et al., *ASM Metals Handbook* (Ninth Edition), American Society for Metals, Vol. II., (1979).